Continental Shelf Research 190 (2019) 103988

Contents lists available at ScienceDirect

Continental Shelf Research

journal homepage: http://www.elsevier.com/locate/csr

Research papers

Coral mortality event in the Flower Garden Banks of the Gulf of Mexico in July 2016: Local hypoxia due to cross-shelf transport of coastal flood waters?

Matthieu Le Hénaff[a,b,*], Frank E. Muller-Karger[c], Vassiliki H. Kourafalou[d], Daniel Otis[c], Kimberley A. Johnson[e], Lucas McEachron[f], HeeSook Kang[d]

[a] University of Miami/Cooperative Institute for Marine and Atmospheric Studies (CIMAS), 4600 Rickenbacker Causeway, Miami, FL, 33149-1098, USA
[b] NOAA Atlantic Oceanographic and Meteorological Laboratory (AOML), 4301 Rickenbacker Causeway, Miami, FL, 33149, USA
[c] University of South Florida, College of Marine Science (USF CMS), 140 7th Avenue South, St. Petersburg, FL, 33701, USA
[d] University of Miami/Rosenstiel School of Marine and Atmospheric Science (RSMAS), 4600 Rickenbacker Causeway, Miami, FL, 33149-1098, USA
[e] NOAA Southeast Fisheries Science Center (SEFSC), 75 Virginia Beach Dr, Miami, FL, 33149, USA
[f] Florida Fish and Wildlife Conservation Commission (FWC), 100 8th Ave SE, St. Petersburg, FL, 33701, USA

ARTICLE INFO

Keywords:
Hypoxia
Coral reef
Upwelling
Shelf processes
Coastal flooding
Connectivity
Ecology

ABSTRACT

Remotely sensed and *in situ* data, in tandem with numerical modeling, are used to explore the causes of an episode of localized but severe mortality of corals, sponges, and other invertebrates at the Flower Garden Banks (FGB) National Marine Sanctuary in July 2016. At about 190 km off the Texas coast, at the top the seamount in the East FGB, up to 82% of coral reef organisms were affected in a 1–2 m thick layer on the local seafloor at ~23 m depth. Analysis of available data pointed to low levels of dissolved oxygen being the most likely contributing factor in the observed mortality (Johnston et al., 2019).

Observations show that upwelling-favorable winds in June and July 2016 carried brackish and turbid coastal waters across the northwestern Gulf of Mexico continental shelf to the FGB. This plume of coastal water was the result of exceptionally high precipitation and local river run-off. Field data provide clear evidence of thin, localized, subsurface near-hypoxic layers immediately below this turbid, low salinity coastal plume. These mid-water layers extended over longer distances (30–40 km), and reached further offshore (~100 km), than previously reported in the region, associated with large quantities of organic matter carried offshore by the brackish plume.

The surface brackish layer was observed to cover the East FGB in satellite ocean color imagery and *in situ* salinity measurements in late June and July 2016. Model results and sparse observations on the shelf suggest that this surface layer was ~20 m thick. It is expected that organic matter carried in the surface layer accumulated on the seafloor of the East FGB, which was just below the brackish plume. In the absence of ventilation, this led to the local formation of a bottom hypoxic layer, similar to what is observed on the Gulf of Mexico inner to mid-shelf every summer.

The conditions experienced at FGB in July 2016 are likely to affect other reefs exposed to brackish plumes with high organic matter loads. The processes of physical connectivity by transport of material is critical for reef colonization and survival, but can also be fatal to coral ecosystems. The monitoring of coral reefs should take the threat of hypoxia due to distant sources of organic matter into account.

1. Introduction

The Flower Garden Banks (FGB) National Marine Sanctuary is located at the Louisiana-Texas (LATEX) shelf break in the northwestern Gulf of Mexico (GoM), between about 110 and 190 km offshore (Fig. 1). It includes three separate sites, namely the East FGB, West FGB, and

---

* Corresponding author. UM/CIMAS, NOAA Atlantic Oceanographic and Meteorological Laboratory (AOML), 4301 Rickenbacker Causeway, Miami, FL, 33149, USA.

E-mail address: m.lehenaff@miami.edu (M. Le Hénaff).

https://doi.org/10.1016/j.csr.2019.103988
Received 19 January 2019; Received in revised form 14 October 2019; Accepted 16 October 2019

Stetson Bank. These small seamounts feature high biodiversity coral reef ecosystems, at depths ranging from $\sim$17 m to $\sim$130 m for the East FGB site (Spalding and Bunting, 2004; Hickerson et al., 2008; Schmahl et al., 2008; Johnston et al., 2019).

On July 25, 2016, SCUBA divers conducting a survey of the East FGB reported the presence of hazy waters and dead invertebrates, including corals and sponges. Sanctuary personnel responded immediately and organized an oceanographic survey in and around the Sanctuary in the following days, in order to characterize the mortality event and determine its origin and cause. The diver survey found that an area of approximately 5.6 ha (2.6% of the coral reef) on the seafloor at the top of the East FGB coral ecosystem, at about 23 m depth, was affected with mortality affecting up to 82% of organisms in a 1–2 m thick band; organisms above this thin layer at the seafloor, or at deeper depths, were not affected (Johnston et al., 2019). The cause of the mortality was not identified at the time. Yet the analysis of the water quality parameters, the patterns of mortality on the reefs, and observations of dissolved oxygen concentrations DO sensors $<$3.5 mg/L at similar depths 50–70 km northwest of East FGB, suggests that the most likely cause for death of organisms was low levels of dissolved oxygen, i.e., hypoxia (Johnston et al., 2019).

The aspect of the organisms affected by the mortality event was similar to that seen during the hypoxia event reported by Altieri et al. (2017) in the Caribbean coast of Panama (Johnston et al., 2019). Altieri et al. (2017) estimated that over 10% of coral reefs around the world are exposed to elevated risks of hypoxia, and that this threat has probably been underreported. However, coral reefs located hundreds of kilometers away from rivers and continental coastal zones, such as the FGB, are generally considered to be safe from such a threat.

Several questions remain about the 2016 FGB mortality event. In particular, what were the regional oceanographic conditions associated with that episode of mortality? What could explain the localized mortality of corals and sponges in a limited depth range at the top of the East FGB, while no similar mortality was observed at the West FGB, only 20 km away? To address these questions, we examined and documented the timeline of physical oceanographic events over the northwestern GoM in the weeks prior to and during the mortality event. Our approach is based on the use of satellite ocean color data, combined with *in situ* measurements and outputs from a realistic model simulation.

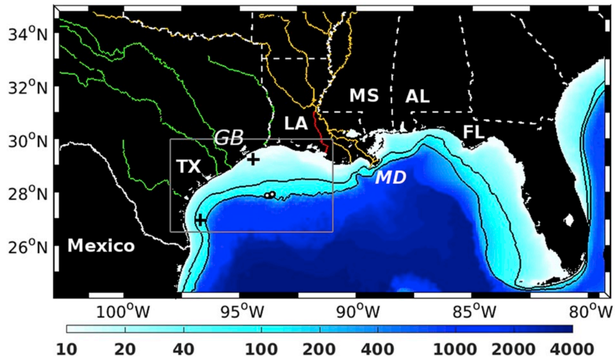

Fig. 1. Bathymetry (m) of the northern Gulf of Mexico (GoM). The white circles with black outlines indicate the locations of the East and West Flower Garden Bank seamounts. The rivers merging to form the Mississippi River are indicated in orange, while the Atchafalaya River is indicated in red. The rivers flowing in the northwestern GoM west of the Mississippi and Atchafalaya Rivers are indicated in green. The border between the U.S. and Mexico is indicated with a solid white line. The borders between the U.S. states are indicated with dashed white lines. States boarding the GoM are labeled as: Texas (TX), Louisiana (LA), Mississippi (MS), Alabama (AL), and Florida (FL). The Mississippi Delta and Galveston Bay are marked with MD and GB, respectively. The black contours represent the isobaths at 50 and 200 m. The black crosses near the coast indicate the locations of the meteorological NOAA NDBC buoys: 42020 (26.97°N; 96.67°W) close to the U.S.-Mexico border, and 42035 (29.23°N; 94.41°W) off Galveston Bay, Texas. The grey frame outlines the focus region of subsequent figures. (For interpretation of the references to color in this figure legend, the reader is referred to the Web version of this article.)

A wide variety of satellite-based remote sensing techniques have been used to examine the distribution and temporal variability of optical characteristics of surface waters of the GoM. Arnone et al. (2017) used imagery from the Visible Infrared Imaging Radiometer Suite (VIIRS) to examine diurnal changes in phytoplankton biomass in the eastern GoM. Schaeffer et al. (2015) evaluated a suite of algorithms to estimate CDOM absorption in estuaries in the northern GoM and found that a reflectance ratio using red and blue bands provided the best fit between field and satellite data. D'Sa et al. (2007) developed a two-band reflectance algorithm based on red and green bands to estimate suspended particulate matter concentrations in the northern GoM. This band ratio is related to the backscattering coefficient at 555 nm. Previous work has demonstrated the utility of ocean color observations to trace physical connectivity patterns in this region (Muller-Karger et al., 1991; Hu and Muller-Karger, 2008; Soto et al., 2009). In this study, we used the Chlorophyll-a product from MODIS and VIIRS to examine temporal patterns of turbid waters that were transported from the coastal GoM to the FGB reefs.

The northwestern Gulf of Mexico (NWGoM), where the mortality event took place, encompasses a wide shelf south of Louisiana and Texas, the LATEX shelf. This shelf is narrow in its western portion near the U.S. and Mexico border, wide in its central part ($\sim$200 km), and narrow again in the east near the Mississippi Delta. Tidal currents at the shelf break are weak ($\sim$3 cm/s), but increase to the north as the shelf gets shallow, reaching about 10 cm/s along the Louisiana coast; they are typically low ($\sim$2 cm/s) close to the U.S.-Mexican border (DiMarco and Reid, 1998). The lower frequency circulation over the inner shelf is mostly driven by winds. Winds are easterly (i.e., from the east) for most of the year, but turn to southerly in summer (Nowlin et al., 2005; Zavala-Hidalgo et al., 2014). As a result, the wind-driven circulation over the LATEX shelf is westward most of the year, with more intense currents near the coast. In summer, this circulation reverses to eastward due to changes in wind direction (Nowlin et al., 2005). Changes in the wind pattern in summer also lead to upwelling along the western coast, near the border between the U.S. and Mexico (Zavala-Hidalgo et al., 2006). The LATEX outer shelf waters are subject to frequent interactions with mesoscale eddies, which are common in the deep GoM (e.g. Biggs and Muller-Karger, 1994; Hamilton et al., 2002). A one-year long survey at the East FGB showed strong inertial currents and weak tidal currents, and confirmed the importance of the wind and eddies in driving the circulation in the FGB area (Teague et al., 2013). Although the East and West FGB form small seamounts, typical physical processes associated with the presence of seamounts, such as Taylor Columns, doming of density surfaces, enclosed circulation cells and enhanced vertical mixing (e.g. White et al., 2007), have not been reported at the FGB to our knowledge.

The mid- and inner LATEX shelf presents widespread hypoxic to anoxic conditions every summer (Rabalais et al., 2002). This is attributed to the decay of phytoplankton blooms and other organic matter associated in great measure with the discharge from the Mississippi and Atchafalaya Rivers (Dale et al., 2007; Conley et al., 2009; Levin et al., 2009). Bacterial consumption of this material and respiration lead to widespread oxygen depletion, which affects the shelf pelagic and benthic ecosystems, leading to stress and mortality of organisms (Rabalais and Turner, 2001). The dynamics of the Mississippi/Atchafalaya River plume plays a major role in the intensity of the hypoxia episodes. Typically, easterly winds strengthen the buoyancy-driven westward river plume circulation along the LATEX shelf. Conversely, southerly winds in the summer favor accumulation of brackish waters west of the Mississippi Delta and eastward advection of waters from the Mississippi and other rivers to the east of the Delta, where they are prone to interacting with the deep GoM current system (Walker et al., 1996; Kourafalou et al., 1996; Muller-Karger et al., 1991, 2015; Muller-Karger, 2000; Morey et al., 2003; Schiller et al., 2011; Androulidakis et al., 2015). Local river discharge and stratification have important effects on the vertical structure of the dissolved oxygen concentration (Hetland and DiMarco, 2008; Bianchi et al., 2010). Although the Mississippi/Atchafalaya system is considered to be the main source of nutrients leading to hypoxia in the NWGoM, other rivers also contribute to hypoxic conditions on the shelf, such as the Brazos River in Texas (DiMarco et al., 2012). Despite the recurrence of hypoxia in coastal and shelf waters of the northern GoM, no hypoxic conditions had previously been reported for the FGB.

The present article is organized as follows: Section 2 describes the data used in our study of the environmental conditions associated with the 2016 mortality event at the East FGB. Section 3 describes the physical conditions and circulation patterns in the NWGoM during June and July 2016, and the vertical structure of the ocean in that region in June 2016, based on observation data. Section 4 provides a discussion of our results, together with our scenario to explain the observed mortality, and presents our conclusions.

2. Data: observations and model simulation

We used ocean color satellite imagery to trace the accumulation and dispersal of turbid coastal waters over the LATEX shelf. Maps of Chlorophyll-a concentration (Chl-a) at 1-km resolution were derived from the Moderate Resolution Imaging Spectroradiometers (MODIS) on NASA's Aqua and Terra satellites (2014 reprocessing) and from the Visible Infrared Imaging Radiometer Suite (VIIRS) on NOAA's Suomi satellite. Level-2 daily satellite pass files for the study region were obtained from NASA's Ocean Biology Processing Group (https://oceancolor.gsfc.nasa.gov/) and subsequently binned to weekly intervals. Chl-a was estimated using NASA's default chlor_a product (Hu et al., 2012; O'Reilly, 2000). We are aware that, in river-dominated coastal and shelf areas, the Chl-a ocean color has a higher uncertainty due to the various other constituents present in the water, including CDOM (e.g. Muller-Karger et al., 1991; Hu et al., 2003; Nababan et al., 2011). However, satellite Chl-a has a lesser level of noise compared to CDOM estimates, which makes it an appropriate choice for tracing the details of the coastal water displacements (Brown et al., 2008; Otis, 2012; Otis et al., 2019). Since ocean color Chl-a estimates have large errors in turbid coastal waters, the Chl-a values presented in this study are not expected to be an accurate estimate of the actual Chlorophyll-a concentration, and we will refer to these values as 'apparent' Chl-a.

Daily satellite-derived Sea Surface Temperature (SST) maps were used to identify coastal upwelling regions where cooler water surfaced near the coast and spread over the shelf. SST maps were extracted from the Multiscale Ultrahigh Resolution (MUR) Sea Surface Temperature dataset from the Group for High Resolution Sea Surface Temperature (GHRSST). The data (2003–2017) were obtained from NASA at a global 0.011° spatial grid. The product amalgamates SST observations from several instruments, including the NASA Advanced Microwave Scanning Radiometer-EOS (AMSRE) and the Moderate Resolution Imaging Spectroradiometer (MODIS).

In situ data were used to complement the remotely sensed data. Wind data were obtained from buoys 42020 and 42035 from NOAA's National Data Buoy Center (NDBC). Buoy 42020 (26.97°N; 96.67°W) is located close to the U.S.-Mexico border, and buoy 42035 (29.23°N; 94.41°W) is off Galveston Bay, Texas (Fig. 1). Surface salinity data was obtained from the Texas Automated Buoy System (TABS) database (TABS, 2018), at buoys V and N located at East and West Flower Garden Banks, respectively. River discharge data for rivers in the region were obtained from the U. S. Geological Survey (USGS) and the U.S. Army Corps of Engineers. Finally, hydrographic sections over the NWGoM shelf were obtained from the June 2016 cruise of the NOAA R/V *Oregon II*. These data included vertical profiles of temperature, salinity, dissolved oxygen concentration, transmissometry (c-beam attenuation coefficient at 660 nm), and fluorometry collected during CTD casts.

In addition to observations, we used outputs from a numerical simulation to investigate certain aspects of the ocean conditions in June and July 2016. We examined hindcasts from our data assimilative, 2 km (1/50°) resolution simulation of the full GoM with the HYbrid Coordinate Ocean Model (GoM-HYCOM 1/50), which has 32 vertical levels (Le Hénaff and Kourafalou, 2016; Androulidakis et al., 2019). The hybrid vertical coordinate system of HYCOM makes it suitable for representing the regional circulation in areas comprising wide continental shelves as well as the deep ocean, such as the GoM (Bleck, 2002; https://hycom.org/). The GoM-HYCOM 1/50 simulation is forced with daily river discharges, implemented at 22 major river mouth locations along the U. S. coasts, including along Texas, while monthly climatological river discharges are represented at minor river mouth locations. The simulation includes detailed representation of river plume dynamics, following Schiller and Kourafalou (2010), and has been used to characterize the episodes of long-distance export of the Mississippi River plume in 2014 (Le Hénaff and Kourafalou, 2016) and in 2015 (Androulidakis et al., 2019). The model assimilates satellite altimetry and SST data, as well as available *in situ* data, in particular salinity and/or temperature profiles from Argo floats and eXpendable Bathy Thermographs (XBT). The simulation is nested at open boundaries into the operational global HYCOM simulation (GLB-HYCOM, hycom.org), and is forced at the surface by the 3-hourly fields from the operational 0.125° resolution ECMWF atmospheric simulation.

3. Results

After the FGB Sanctuary staff contacted us shortly after divers reported the mortality event, we examined the series of apparent Chl-a images to analyze how the spatial patterns of turbid coastal and clear offshore ocean waters changed over time, prior to and during the event.

Leading up to the event, weekly composites of apparent Chl-a images show large quantities of high apparent Chl-a waters along the NWGoM coast throughout June 2016 (Fig. 2). During June 3–9, a wide band (~130 km) of high apparent Chl-a extended along the entire coast of Texas. This pattern is not typical for this time of the year, as shown by the positive anomalies in apparent Chl-a with respect to the 2003–2010 climatology (Fig. 3). Along the coast of Louisiana, in the northeast part of the domain, a narrow band (~60 km) of high apparent Chl-a was observed on these dates (Fig. 2). However, this band was associated with negative apparent Chl-a anomalies (Fig. 3), meaning that the apparent Chl-a was lower than the climatological values in June 2016. This latter pattern also occurred in May 2016 (not shown), suggesting that the Mississippi and Atchafalaya Rivers (in orange and red on Fig. 1) had only a limited influence in this area in the spring of 2016, compared to previous years.

The unusual spatial distribution of coastal river waters in the spring of 2016 off Texas is in part explained by the time series of river discharge in the region (Fig. 4). Although the discharge of the Mississippi and Atchafalaya Rivers was high in the first quarter of 2016, these rivers showed lower discharge in the ensuing spring and summer, close to or below climatological values. On the other hand, the smaller rivers discharging into the NWGoM (in green on Fig. 1) showed sustained and large discharge values from April to June, with combined peak values near 10,000 m^3/s, or 5 to 10 times larger than usual. This was the result of the intense local rains and floods that occurred during this period (Breaker et al., 2016). The cumulative discharge of these rivers in early June was equivalent to the discharge of the Atchafalaya River, and half of the Mississippi River discharge, for this time period.

Between June 3–9 and June 17–23, the broad band of high apparent Chl-a along the Texas coast expanded offshore (Fig. 2). During June 17–23, the brackish waters covered roughly two thirds of the distance between the Texas coast and the FGB. In the following 7-day period, from June 24 to 30, the band of high apparent Chl-a waters continued extending offshore and almost reached the FGB sites from the northwest (Fig. 2).

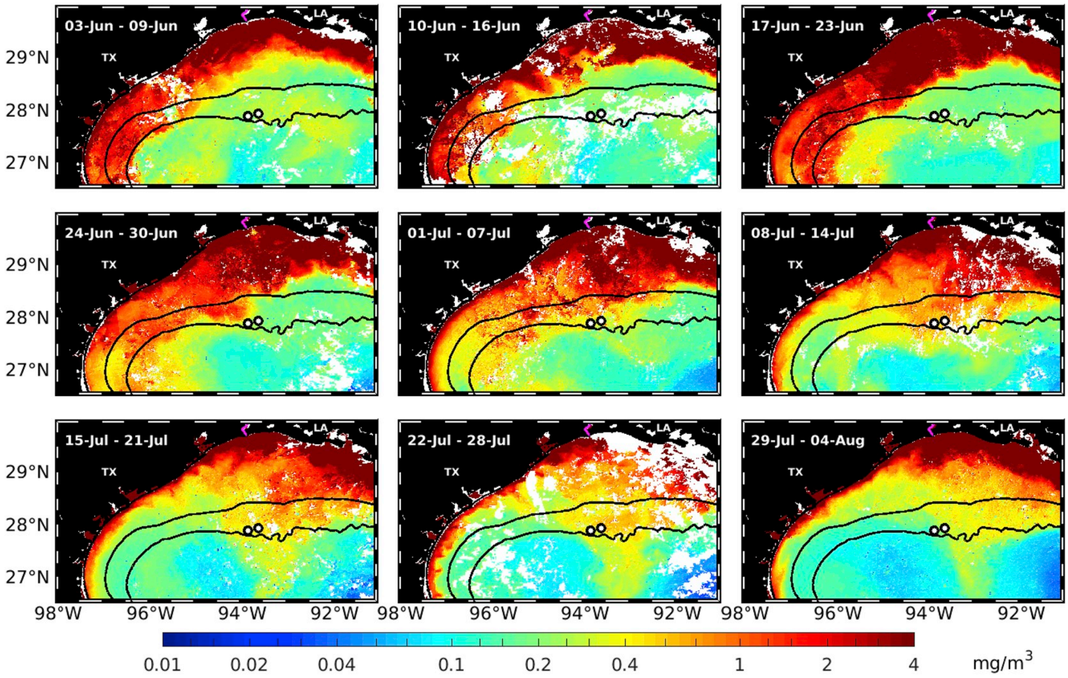

Fig. 2. Temporal evolution of the offshore extension of surface brackish waters using Chlorophyll-a. Weekly composites of the apparent Chlorophyll-a concentration (Chl-a, mg/m^3) from MODIS-Aqua from June 3–9 to July 29 - August 4, 2016. The black contours represent the isobaths at 50 and 200 m. The white circles with black outlines indicate the locations of the East and West FGB sites. The state border between Louisiana (LA) and Texas (TX) is indicated with a magenta line.

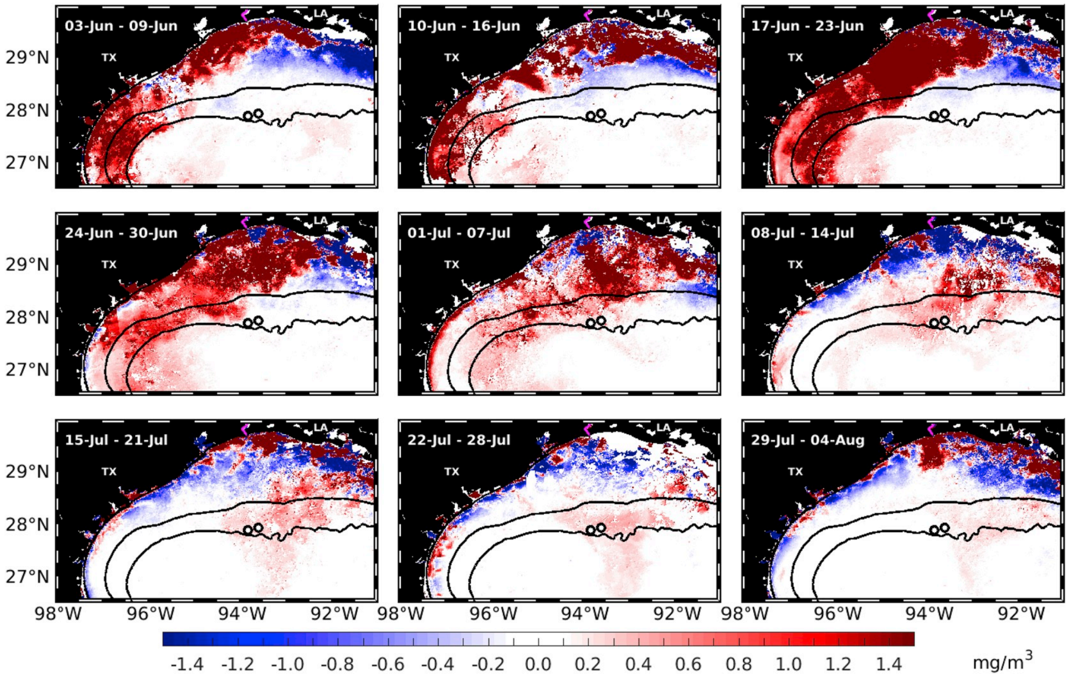

Fig. 3. Temporal evolution of the offshore extension of surface brackish waters using Chl-a anomalies. Weekly composites of apparent Chl-a anomaly with respect to the 2003–2010 climatology (mg/m^3) from MODIS-Aqua from June 3–9 to July 29 - August 4, 2016. The black contours represent the isobaths at 50 and 200 m. The white circles with black outlines indicate the locations of the East and West FGB sites. The state border between Louisiana (LA) and Texas (TX) is indicated with a magenta line.

During July 1–7 and July 8–14, the high apparent Chl-a waters reached the FGB area. Apparent Chl-a values along the coast of the LATEX shelf decreased markedly at this time (Figs. 2 and 3). Indeed, the large pool of coastal, turbid waters observed there in June had been advected offshore, reaching the FGB. After July 8–14, the apparent Chl-a at the edge of the shelf break around the FGB decreased, but the FGB sites remained affected with high apparent Chl-a until July 29 – August 4 (Figs. 2 and 3). By that time, the high apparent Chl-a event that affected the FGB had subsided (Fig. 3).

Fig. 5 presents the wind vectors for June and July 2016 at two buoys located on the LATEX shelf (see Fig. 1). The vector plots show two episodes of sustained upwelling-favorable winds along the coast. These

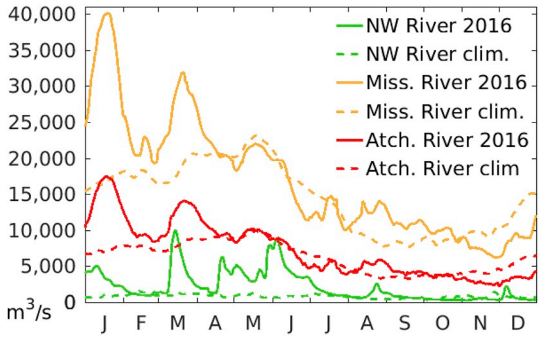

Fig. 4. Temporal evolution of river discharge in the northern Gulf of Mexico in 2016. 2016 river discharge time series (m^3/s) for the combined northwestern Gulf of Mexico rivers in green (Sabine, Neches, Village Creek, Trinity, San Jacinto, Brazos, Lavaca, Guadalupe, and San Antonio rivers), the Mississippi River in yellow, and the Atchafalaya River in red. Solid lines show 2016 values; dashed lines show climatological values (2004–2014). (For interpretation of the references to color in this figure legend, the reader is referred to the Web version of this article.)

two periods are highlighted in red. First, from June 12 to 18, southerly winds blew along the southern coast of Texas adjacent to Mexico (~27°N, ~96.5°W, Fig. 5a), i.e. almost parallel to the coast at that location (Fig. 1). This favored eastward, offshore export of coastal waters through Ekman transport (Zavala-Hidalgo et al., 2006). Within two days, intense southwesterly winds also blew in the region off Galveston (~29°N, ~94.5°W, Fig. 5b), almost parallel to the coast, thus also favoring upwelling there. This wind event coincided with the initial offshore export of turbid coastal waters (Figs. 2 and 3). Analysis of the daily apparent Chl-a images shows that, from June 10 to June 16, the offshore front of the coastal waters advanced ~50 km over 6 days, or an average ~0.1 m/s.

In July, intense, sustained winds were observed at both NWGoM stations for the first half of the month (from July 2 to 17), with the most intense winds in the July 3–10 period. Like in June, these were dominantly southerly along southern Texas, and southwesterly off Galveston, so that the winds were upwelling-favorable along the entire Texas coast. These winds thus also favored the offshore advection of the turbid, brackish coastal waters. By mid-July, apparent Chl-a values along the coast of the LATEX shelf decreased markedly (Figs. 2 and 3) as the large pool of coastal, turbid waters observed there in June had been advected offshore. Between July 2 and July 4, the front moved rapidly, over ~40 km, corresponding to a ~0.2 m/s velocity. Then, the leading front of coastal waters slowed down, but still advanced an additional ~40 km through July 12. On average, between July 2 and July 12, the front advanced at ~0.1 m/s.

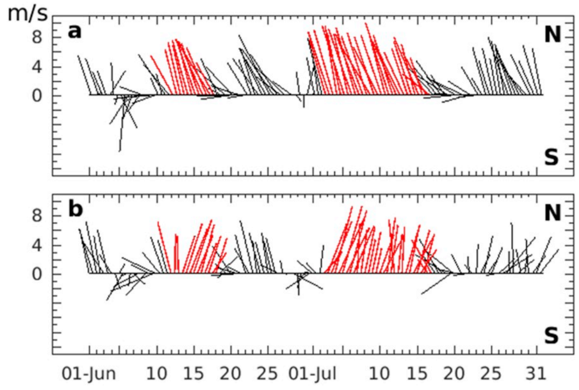

Fig. 5. Wind conditions along the Texas coast in June and July 2016. (a) 10-m wind vectors (m/s) at NDBC station 42020 located at (26.97°N; 96.67°W) every 12 h for June and July 2016. In red are the wind vectors in June 12–18 and July 2–17, during the upwelling events (see text). (b) same as (a) at the NDBC station 42035 located at (29.23°N; 94.41°W). The upward direction is the north (marked with N), the downward direction is the south (marked with S). (For interpretation of the references to color in this figure legend, the reader is referred to the Web version of this article.)

The upwelling in mid-June and early July 2016 was confirmed by examination of the weekly satellite-derived SST observations (Fig. 6). Although upwelling is common in summer in the western GoM (Zavala-Hidalgo et al., 2006), the events described here led to especially widespread cool sea surface temperatures, particularly in July 2016, extending from Mexico as far as Galveston Bay (Fig. 6b). The coastal upwelling of June and July 2016 led to the offshore advection of the river waters that had accumulated along the coast in the spring of 2016.

We now focus on the detailed timeline of the influence of coastal river waters on the FGB. Fig. 7a presents the time series of the surface apparent Chl-a levels above both FGB sites, derived using the daily instantaneous estimates from MODIS (Aqua and Terra) and VIIRS, as well as climatological apparent Chl-a values. We checked that the observations from each satellite source were consistent with one another during our study period before blending them into a single, multi-sensor apparent Chl-a time series. The time series provided exceptional coverage, in complement to the weekly composites shown in Figs. 2 and 3. In particular, it shows that the largest apparent Chl-a values above the FGB were reached on July 2nd, when the front of turbid brackish waters reached the FGB locations for the first time. The peak in surface apparent Chl-a values is short, and apparent Chl-a values decreased over the following days. Before the peak, in June, the values at both sites were lower than the climatological values. After the peak, the apparent Chl-a values remained higher than climatological values, and increased again after July 5. The values of surface apparent Chl-a at both FGB sites were similar throughout June and July until July 13. After July 13, surface apparent Chl-a at East FGB was larger than at West FGB until the end of July. Between July 13 and 22, surface apparent Chl-a at East FGB reached 0.4–0.5 mg/m^3, more than twice the climatological value, in the period directly preceding the observation of the mortality. The positive surface apparent Chl-a for this period was smaller than the one around

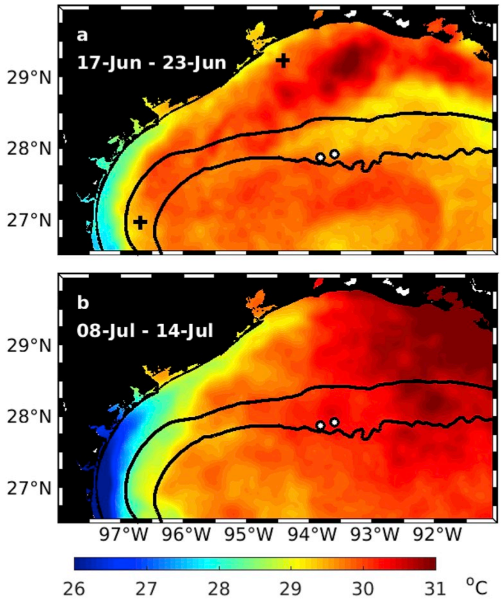

Fig. 6. Evidence of upwelling along the Texas coast in June and July 2016 based on Sea Surface Temperature maps. Weekly averages of Sea Surface Temperature (°C) from the GHRSST dataset for: (a) June 17–23; (b) July 8–14, 2016. The black contours represent the isobaths at 50 and 200 m. The white circles with black outlines indicate the locations of the East and West FGB sites. The black crosses near the coast indicate the locations of the meteorological NDBC buoy stations 42020 and 42035 (see also Fig. 1).

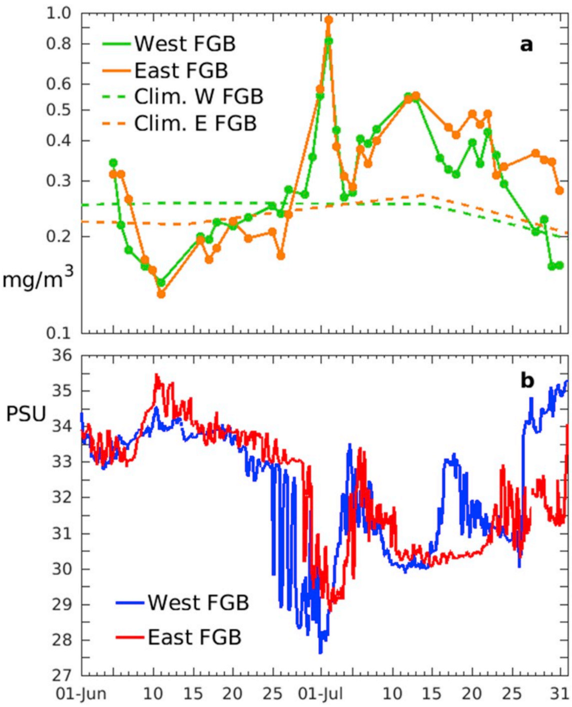

Fig. 7. Signature of the presence of surface brackish waters at the FGB locations. (a) Time series of apparent Chl-a (mg/m^3) at the surface above the West FGB site (green) and the East FGB site (orange) in June and July 2016, based on MODIS Aqua, MODIS Terra, and VIIRS (solid lines). The 2003–2010 climatological monthly values (mg/m^3) estimated from MODIS-Aqua are indicated for reference (dashed lines). (b) Time series, in June and July 2016, of surface salinity (PSU) above the West FGB site (blue) and the East FGB site (red) from the TABS buoy data. (For interpretation of the references to color in this figure legend, the reader is referred to the Web version of this article.)

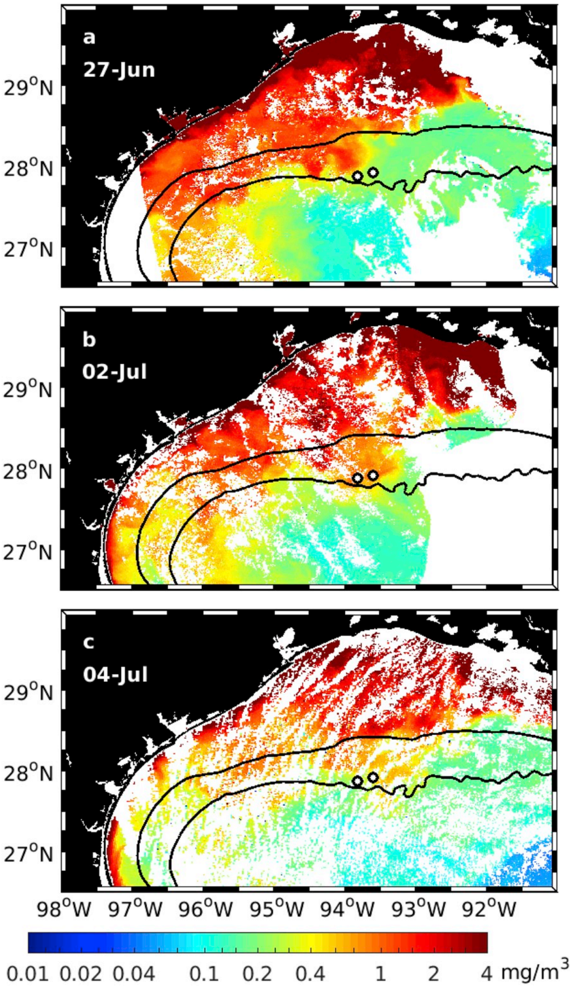

Fig. 8. Spatial patterns in surface apparent Chl-a observed during the first Chlorophyll-a peak observed above both East and West FGB sites in late June and early July 2016. Apparent Chl-a (mg/m^3) observed on: (a) June 27, 2016 at 18:05 UTC by MODIS-Aqua, (b) July 2, 2016, at 15:15 UTC by MODIS-Terra, and (c) July 4, 2016, at 16:40 UTC, by MODIS-Terra. The black contours represent the isobaths at 50 and 200 m. The white circles with black outlines indicate the locations of the East and West FGB sites.

July 2 but it lasted longer at East FGB.

Fig. 7b presents the hourly surface salinity observed above both East and West FGB sites. These observations are consistent with the surface apparent Chl-a time series (Fig. 7a). Low salinity waters reached both the East and West FGB locations in late June, with a peak around July 2. Surface salinity in late June and early July was lower at West FGB than at the East FGB, and the influence of coastal waters lasted longer at West FGB than at East FGB during that period. After July 2nd, the salinity time series show, like for the surface apparent Chl-a, a decrease of the influence of coastal waters, marked with an increase in salinity at both sites, before a second period of influence of coastal waters. As for the apparent Chl-a, that second period is less marked than the one around July 2nd, but it lasted longer at East FGB. From July 10 to 22, the surface salinity at East FGB remained constantly below 31, indicating a prolonged period of presence of the brackish coastal waters atop the East FGB.

Fig. 8 illustrates the spatial patterns in apparent Chl-a observed in late June and early July 2016, when the first peak in apparent Chl-a was observed above both East and West FGB sites (Fig. 7). On June 27 (Fig. 8a), the band of coastal waters, which had been extending from the coast (Fig. 2), formed a bulge extending southeastward, reaching close to the FGB sites and partially affecting the West FGB site (Fig. 7b). On July 2 (Fig. 8b), this bulge extended further southeastward and covered both FGB sites. On July 4 (Fig. 8c), it had recessed and the apparent Chl-a at FGB sites was lower than in the waters to the north and east of the sites. These patterns explain the short peak observed in surface apparent Chl-a on July 2 (Fig. 7a) at both FGB sites.

Fig. 9 provides more details about the situation in mid to late July. On July 13 (Fig. 9a), the surface plume of coastal waters covered the central and eastern parts of the LATEX shelf and its southward extension covered both FGB sites. Within these coastal waters, a filament of more intense apparent Chl-a was located just north of the East FGB site. On July 20 (Fig. 9b), the spatial distribution of the coastal waters in the NWGoM was similar, although apparent Chl-a was somewhat lower relative to July 13. A portion of the coastal, high apparent Chl-a waters was also entrained south of the FGB to the deep GoM. Waters with larger apparent Chl-a were located to the north and northeast of the East FGB site, which explains the larger surface apparent Chl-a and lower salinity at East FGB than at West FGB at that time (Fig. 7). This pattern is more visible on July 22 (Fig. 9c), when a patch of higher apparent Chl-a covered the East FGB site but not the West site. The maps of apparent Chl-a explain the higher surface apparent Chl-a and lower salinity at the East FGB site than at the West FGB site during July 13–22 (Fig. 7).

We now investigate the vertical structure of the upper ocean over the LATEX shelf, by analyzing the *in situ* observations of salinity, temperature, density, dissolved oxygen, and chlorophyll concentration in the water column, collected by the R/V *Oregon II* in June 2016 (Fig. 10). A hydrographic section centered at about 93.7°W, east of Galveston Bay (~94.5°W), was constructed from samples collected during June 23–26 (blue dots in Fig. 10a). That section was constructed artificially by using data collected from the ship over a 3-day period. Since the maximum velocity of the surface coastal water front in June was estimated to be

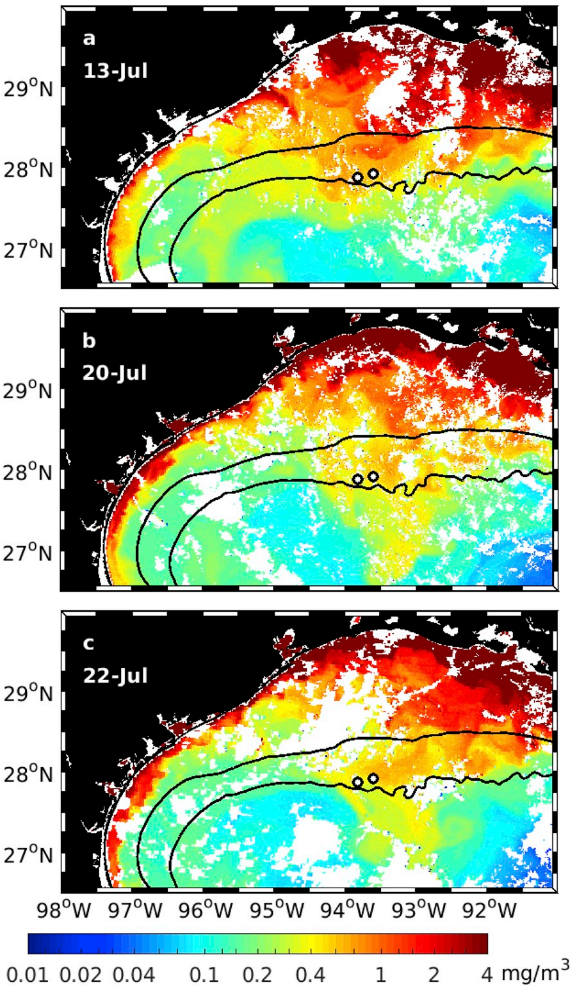

Fig. 9. Spatial patterns in surface apparent Chl-a observed during the second Chlorophyll-a peak observed above the FGB sites in mid to late July 2016. Apparent Chl-a (mg/m^3) observed by MODIS-Terra on: (a) July 13, 2016 at 16:35 UTC, (b) July 20, 2016, at 16:40 UTC, and (c) July 22, 2016, at 16:30 UTC. The black contours represent the isobaths at 50 and 200 m. The white circles with black outlines indicate the locations of the East and West FGB sites.

~0.1 m/s, this corresponds to a maximum displacement of the front of ~26 km during the three-day observation period, which is much smaller than the total length of section (189 km). We are thus confident that this section represents a near synoptic view of the vertical structure through the plume of coastal waters.

The hydrographic section spans the initial offshore expansion of the turbid coastal river plume following the mid-June upwelling. The cross-shelf section of salinity and temperature (Fig. 10b) shows a brackish water plume extending from the surface to 5–10 m depth, and from the coast southward to about 28.5°N. This agrees with the front of high apparent Chl-a observed in the satellite data (Fig. 10a). Salinity within the brackish water layer was as low as 22. A marked density gradient (Fig. 10c, contours) was observed at the bottom of the buoyant plume. Fig. 10c shows a marked dissolved oxygen deficit immediately below the surface layer of brackish waters, which are marked with low salinity and high apparent Chl-a. Dissolved oxygen values in the subsurface tongue spreading offshore were <3 mg/L (hypoxic waters are usually defined with values < 2 mg/L). Outside this thin layer, values were larger than 6 mg/L.

Layers of dissolved oxygen minima are not uncommon below a river plume. These are typically observed in the large hypoxic region of the northern GoM on the LATEX shelf in summer. Zhang et al. (2015) observed such mid-water oxygen minimum layers south of Atchafalaya Bay (~92°W) and south of the Mississippi Delta extending offshore 20–25 km. They show that such low oxygen layers can be continuous and that they track the bottom boundary layer, where the pycnocline intersects the bottom. The low oxygen layers basically detach from the bottom layer and follow the pycnocline offshore.

In June 2016, the mid-water layer of low dissolved oxygen extended southward 30 to 40-km, reaching 100 km from the coast. This is further offshore than had previously been observed in the NWGoM by Zhang et al. (2015, ~65 km). This low oxygen layer was associated with high turbidity (low light-transmission) and high relative chlorophyll fluorescence. Its position, immediately below the surface plume of brackish waters (Fig. 10d) indicates that particles containing chlorophyll were sinking from the surface plume and accumulating at the pycnocline. Phytoplankton and other associated organic particles sink and become trapped in such density layers. Unable to photosynthesize in the dark under the plume, the phytoplankton decomposed along with organic matter advected from the coast. This bacterial activity led to the low oxygen observed.

A similar low oxygen layer below the surface brackish plume was observed along a second near-synoptic section from the R/V *Oregon II* cruise around ~94.9°W, southwest of Galveston Bay, between June 16 and 18 (Fig. 11). There, the low-salinity surface layer extended to 10–15 m depth, with a salinity value of 26. Below this surface layer, a very thin layer of low oxygen, with values as low as 3.5 mg/L, extended offshore over a 30–40 km distance. This layer was also associated with low light transmission and high chlorophyll fluorescence.

The evidence of cross-shelf low oxygen mid-water layers under an eastward-southeastward propagating surface brackish layer over the LATEX shelf shows that such layers can form not only under the Mississippi/Atchafalaya plume, as observed previously (Zhang et al., 2015), but also under a surface layer to which small, local NWGoM rivers contributed significantly. This complements the identification of near-shore hypoxia forced by the Brazos river along the Texas coast (DiMarco et al., 2012).

4. Discussion and conclusions

Our results confirm that the FGB mortality event of July 2016 occurred after the turbid coastal waters, which accumulated in the spring of 2016 after precipitation and river discharge excess along the Texas coast, were advected offshore by upwelling favorable winds. During that process, as we just described, mid-water layers of low oxygen were observed to extend about half-way on the shelf in June, which is remarkable. Such a mid-water layer of very low oxygen values (hypoxic waters), comparable to the ones observed in June 2016, intersecting the underwater reefs at FGB could be fatal to corals and sponges. However, the other vertical profiles collected in June 2016 do not show the presence of these mid-water layers of low oxygen, which suggests that these layers were patchy and localized. In addition, although these mid-water layers extended far offshore on the LATEX continental shelf, their extent was still another ~90 km away from the FGB sites. As the surface layer of brackish waters extended further offshore, its bottom was more prone to being ventilated from below in open shelf conditions, so that it is unlikely that the level of oxygen could be maintained at very low levels as far offshore as the FGB sites. These considerations make it unlikely that a mid-water filament of hypoxic waters directly impacted the East FGB.

However, the presence of mid-water layers of low oxygen so far offshore as observed in June 2016 illustrates the very large quantities of organic matter that were entrained offshore, which made the surface layer of brackish waters prone to developing a low-oxygen layer at its base. As the surface layer of brackish waters reached the FGB seamounts, it found a portion of seafloor at a shallow depth, ~23 m at East FGB (17 m is the shallowest part of the seamount, 23 m is the seafloor, Johnston et al., 2019).

In order to characterize the vertical extent of the brackish plume in

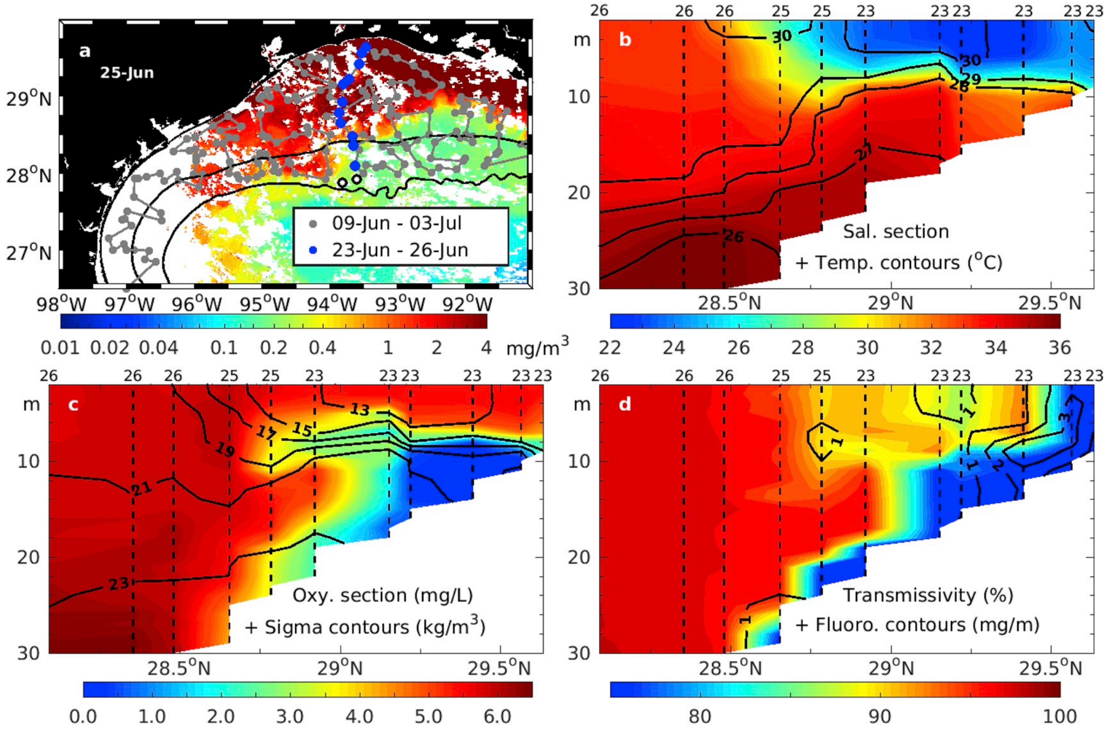

Fig. 10. Evidence of a mid-water layer of low oxygen waters extending offshore in the NWGoM in June 2016. (a) Apparent Chl-a (mg/m3) observed by MODIS-Aqua on June 25, 2016 at 18:20 UTC. Superimposed are the locations of the in situ samples from the R/V Oregon II collected from June 9 to July 3, 2016. The blue dots represent a virtual track constructed from stations of the actual cruise track (in grey dots and lines) occupied between June 23-26. The black contours represent the isobaths at 50 and 200 m. The white circles with black outlines indicate the locations of the East and West FGB sites. (b-d) Vertical sections, along the virtual track (blue dots) shown in (a), of: (b) salinity (colors) and temperature (contours, °C), (c) dissolved oxygen (colors, mg/L) and sigma density anomalies (contours, kg/m^3), (d) transmissivity (colors, %) and chlorophyll fluorometry (contours, mg/m). (b-d) The vertical sections are linearly interpolated between the individual vertical profiles collected during the cruise. The vertical dashed black lines mark the locations of in situ measurements. The day of the month (June) at which these measurements were taken is marked at the top of each vertical dashed line. (For interpretation of the references to color in this figure legend, the reader is referred to the Web version of this article.)

July, at the period when the mortality took place, we use outputs from the GoM-HYCOM 1/50 model simulation (see Section 2), with realistic river forcing and data assimilation, on July 22, 2016 (Fig. 12). The simulated sea surface salinity (Fig. 12a) shows very similar patterns as those observed on apparent Chl-a on the same day (Fig. 9c): first, the core of the brackish and fresh plume is located on the northern part of the shelf, and the plume extends over the shelf to the south; then, although their location slightly differs, both the observations and the simulation show filaments of waters with stronger riverine signature (large apparent Chl-a or low salinity) just north of the FGB sites; finally, filaments of low-salinity, riverine waters were exported south of the shelf break near the FGB sites in the simulation, similar to observations. The salinity of the surface waters reaching East FGB was ~33 in the simulation, compared to ~31 in the observations on July 22 (Fig. 7). Despite these differences, the simulation is able to represent the offshore export of brackish waters in July 2016 over the NWGoM shelf in a realistic manner. The vertical structure of the simulated brackish plume extended to ~20 m depth on the outer part of the shelf, including in the FGB area (Fig. 12b). This model estimate is in agreement with limited observational data sampled on the LATEX shelf in July 2016, which show that the low-salinity surface layer extended to ~20 m depth (S. DiMarco, personal communication). *In situ* data from the U.S. Geological Survey showed low values of subsurface dissolved oxygen at a couple sites on the LATEX shelf, at similar depths as the East FGB top, in late July and early August 2016 (Johnston et al., 2019). These observations also suggest that the surface layer of brackish waters extended to ~20 m depth; they also suggest that mid-water layers of low oxygen were also present on the shelf in July 2016, stressing again the large quantities of organic matter exported in the surface layer.

We expect that the presence of brackish waters just over the seamount cap led to the accumulation of organic matter on the seafloor. As is happening on the LATEX upper-shelf in summer, a layer of highly turbid waters present at the top of the seamount would be isolated between the seafloor and the strong stratification at the base of the surface, low-salinity waters. This would severely inhibit the ventilation of the bottom layer, favoring hypoxia (Rabalais et al., 2002; Rabalais and Turner, 2001). This process is consistent with the patterns of the mortality reported during the assessment dives in late July and early August 2016, with the affected organisms located at the base of coral structures and in sand channels between them (Johnston et al., 2019).

In addition to the shallow seafloor at the top of the FGB seamounts, coral structures at the top of the seamounts themselves might also have favored retention of organic matter. Indeed, immerged corals are often seen as a canopy that slows down the current near the bottom, especially under limited wave influence as expected at the depth of the FGB sites (Nepf and Vivoni, 2000; Nepf, 2012; Lowe and Falter, 2015; Pomeroy et al., 2017). Moreover, large coral structures were also found to slow the current at their base, which favored coral bleaching in lagoons of Moorea, French Polynesia (Lenihan et al., 2008). In general, low-velocity flow conditions around corals favor bleaching (Nakamura and van Woesik, 2001; Nakamura et al., 2005) and hypoxia (Brown and Carpenter, 2013). The coral structures at the top of the East FGB, as they tend to reduce the velocity of the flows near the seafloor, thus favored the accumulation of organic matter deposited from the surface brackish waters. Although it is not possible, with the existing data, to confirm that such small-scale dynamical processes played a significant role at East FGB, they might also have contributed to the local formation of low oxygen waters.

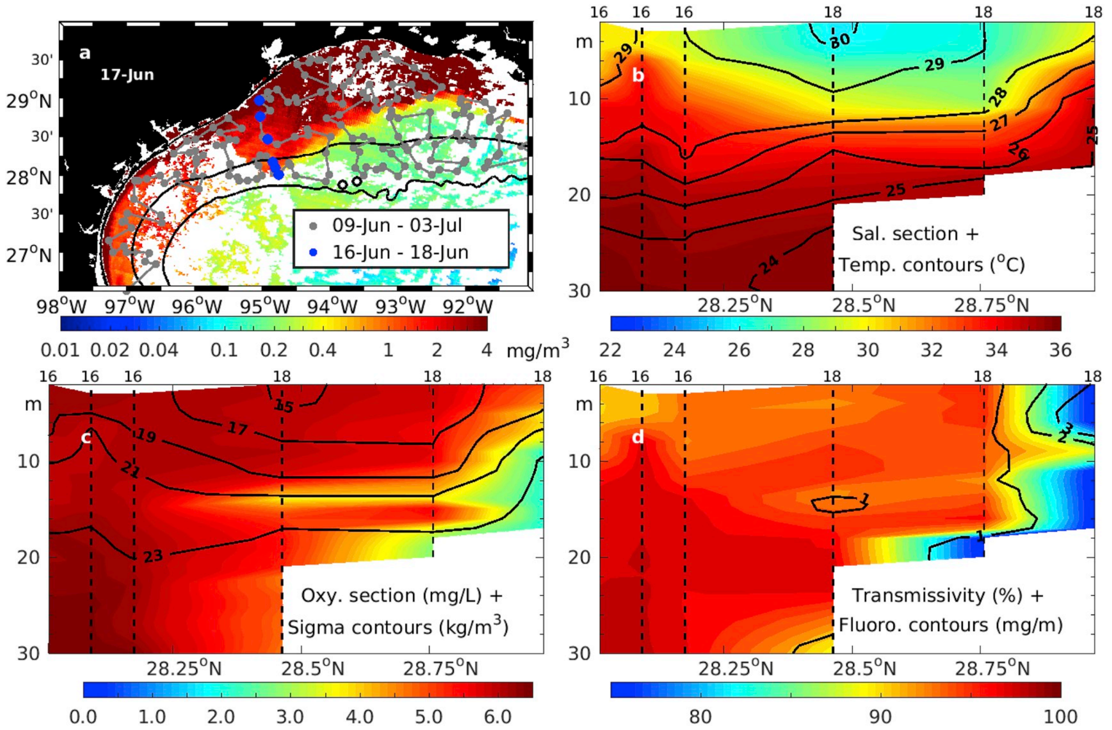

Fig. 11. Same as Fig. 10, for the virtual section indicated in blue dots in (a), for data collected between June 16 and 18, 2016. (a) Apparent Chl-a (mg/m3) observed by MODIS-Terra on June 17, 2016 at 16:00 UTC. (For interpretation of the references to color in this figure legend, the reader is referred to the Web version of this article.)

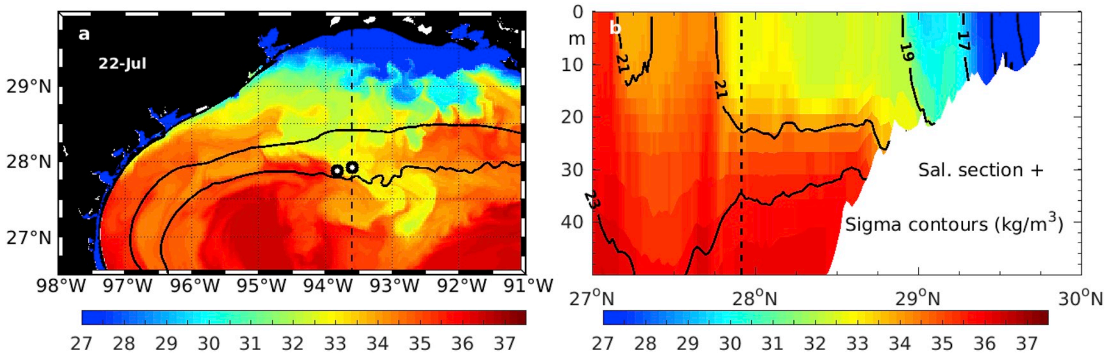

Fig. 12. Spatial and vertical extent of the simulated plume of brackish waters on July 22, 2016. (a) Simulated sea surface salinity (PSU) on July 22. The black contours represent the isobaths at 50 and 200 m. The white circles with black outlines indicate the locations of the East and West FGB sites. (b) Vertical section (in m of depth), along the meridional dashed line at the longitude of East FGB shown in (a), of salinity (colors) and sigma density anomalies (contours, kg/m^3). The vertical dashed line marks the location of East FGB. (For interpretation of the references to color in this figure legend, the reader is referred to the Web version of this article.)

The time series of surface apparent Chl-a and salinity above both FGB sites (Fig. 7) and the evolution of the spatial extent of the surface layer of coastal waters (Fig. 9) might explain why the East FGB site was the only one affected. Indeed, surface apparent Chl-a values were larger, and salinity was lower, at East FGB than at West FGB for a prolonged period of time between July 13 and 22 (Fig. 7). This indicates that the presence of river waters was more marked at East FGB site compared to West FGB, which suggests that: 1) the stratification at the base of the surface layer was more intense; 2) the organic matter content was higher. Both processes make the local formation of a low oxygen layer at the top of the East FGB seamount more likely than at the West FGB site.

The fact that the presence of brackish waters at both FGB sites in late June/early July, with more pronounced anomalies in apparent Chl-a and salinity than later in July, did not lead to mortality might be due to the duration of that initial peak, which was shorter than the one in mid-July. During laboratory experiments, Altieri et al. (2017) found that corals exposed to hypoxic conditions died in less than 7 days, while Haas et al. (2014) observed complete coral mortality of corals in hypoxic conditions in about 3 days. Whereas the initial peak in late June/early July might have led to hypoxic conditions, they might not have prevailed for a long enough time to lead to mortality, whereas the prolonged presence, at East FGB, of the brackish waters from July 10 to 22 appears more favorable.

The absence of mortality during the short presence of brackish waters in late June/early July might also be due to dynamical conditions, as quiescent conditions would likely be necessary to retain the organic matter at the top of the seamount. Such quiescent conditions might have been favored by the coral structures at the top of the FGB sites. A high-resolution, coupled physics-biogeochemistry model, with adapted drag coefficient on the top of the seamount to represent the effect of the corals, will be necessary to further study the physical and biogeochemical processes that led to the coral mortality at East FGB.

The offshore export of low-salinity, riverine waters over the NWGoM continental shelf, which we describe in detail in the Results section, thus provided favorable conditions for the local formation of a layer of low-oxygen waters at the top of the East FGB seamount, which were reported to be the most likely contributing factor in the reported mortality of corals and sponges (Johnston et al., 2018). The expansion, in the summer of 2016, of riverine waters on the NWGoM shelf over such a wide area was exceptional. The event was associated with the extremely large amount of fresh water discharged by small Texas rivers onto the NWGOM shelf in early summer 2016, which was due to unusually high precipitation in spring. This extreme precipitation in 2016 followed intense precipitation in 2015, which was also associated with large river discharge into the GoM (Fournier et al., 2016), although no distant hypoxia was reported that year.

The results presented here help understand the anomalous coral and sponge mortality event of 2016 at FGB. As high local precipitation, combined with winds favoring the offshore transport of coastal waters, can episodically occur, our study findings should be beneficial to the design of future monitoring plans. Moreover, these findings suggest that similar processes might affect other coral reefs worldwide, especially those located near known hypoxic zones (Altieri et al., 2017). Coastal freshwater discharge conditions and the variability of the plumes they generate should be monitored routinely to differentiate between various processes that impact the health of coral reef ecosystems, even those at large distances from the coast.

Declaration of competing interest

The authors declare that they have no known competing financial interests or personal relationships that could have appeared to influence the work reported in this paper.

Acknowledgements

This paper is a result of research funded by the National Oceanic and Atmospheric Administration RESTORE Act Science Program under award NA15NOS4510226 to the University of Miami. It is a contribution to the Marine Biodiversity Observation Network (MBON) program. The work was partially supported by NASA grant NNX14AP62A 'National Marine Sanctuaries as Sentinel Sites for a Demonstration Marine Biodiversity Observation Network (MBON)' funded under the National Ocean Partnership Program (NOPP RFP NOAA-NOS-IOOS-2014-2003803 in partnership between NOAA, BOEM, and NASA), and the NOAA Integrated Ocean Observing System (IOOS) Program Office. M. Le Hénaff received partial support for this work from the base funds of the NOAA Atlantic Oceanographic and Meteorological Laboratory and was supported in part under the auspices of the Cooperative Institute for Marine and Atmospheric Studies (CIMAS), a cooperative institute of the University of Miami and NOAA, cooperative agreement NA10OAR4320143. The Chlorophyll-a data were derived from ocean color images collected by the NASA Moderate Resolution Imaging Spectroradiometer (MODIS), were obtained from NASA's Ocean Biology Processing Group, and were further processed and distributed by the University of South Florida's Institute for Marine Remote Sensing (http://data.imars.marine.usf.edu). The MUR Global High-Resolution SST dataset is distributed by NASA (http://podaac.jpl.nasa.gov/dataset/JPL-L4UHfnd-GLOB-MUR). The NOAA National Data Buoy Center data are publicly available (www.ndbc.noaa.gov). The river discharge data from USGS and the Army Corps of Engineers are distributed by the Gulf of Mexico Coastal Ocean Observing System (GCOOS, http://gcoos.tamu.edu/products/index.php/waterquality/river-discharge-data/). The R/V *Oregon II* cruise in June 2016 was supported by a collaboration between the NOAA National Marine Fisheries Service (NMFS) and the Southeast Area Monitoring and Assessment Program (SEAMAP) in the GoM. The cruise data are publicly available on the NOAA Nationial Centers for Environmental Information portal (https://www.ncei.noaa.gov/), in the Oceans dataset. We thank L. Johns for useful suggestions that improved the manuscript. We are grateful to G. Schmahl, E. Hickerson, S. Gittings, and G. Sedberry of the NOAA National Marine Sanctuaries for their insightful comments in discussions leading to this manuscript. We are grateful to S. DiMarco of Texas A&M University for sharing observation data. We are grateful to the Flower Garden Banks National Marine Sanctuary managers, in particular M. Johnston, for fruitful discussions and their interest in the unique episode discussed herein, which led to organizing the 2016 Flower Garden Banks Localized Mortality Event Mini-Symposium (Galveston, TX, February 27–28, 2018). We thank two anonymous reviewers for their help in improving our manuscript.

References

Schiller, R.V., Kourafalou, V.H., Hogan, P., Walker, N.D., 2011. The dynamics of the Mississippi River plume: impact of topography, wind and offshore forcing on the fate of plume waters. J. Geophys. Res. 116 (C6). C06029.

Altieri, A.H., Harrison, S.B., Seemann, J., Collin, R., Diaz, R.J., Knowlton, N., 2017. Tropical dead zones and mass mortalities on coral reefs. Proc. Natl. Acad. Sci. U.S.A. 114 (14), 3660–3665.

Androulidakis, Y.S., Kourafalou, V.H., Schiller, R., 2015. Process studies on the Mississippi River plume: impact of topography, wind and discharge conditions. Cont. Shelf Res. 107, 33–49. https://doi.org/10.1016/j.csr.2015.07.014.

Androulidakis, Y., Kourafalou, V.H., Le Hénaff, M., Kang, H.-S., Sutton, T., Chen, S., Hu, C., Ntaganou, N., 2019. Offshore spreading of Mississippi waters: pathways and vertical structure under eddy influence. J. Geophys. Res. 124, 5952–5978.

Arnone, R., Vandermuelen, R., Soto, I., Ladner, S., Ondrusek, M., Yang, H., 2017. Diurnal changes in ocean color sensed in satellite imagery. J. Appl. Remote Sens. 11 (3).

Bianchi, T.S., DiMarco, S.F., Cowan, J.H., Hetland, R.D., Chapman, P., Day, J.W., Allison, M.A., 2010. The science of hypoxia in the Northern Gulf of Mexico: a review. Sci. Total Environ. 408 (7), 1471–1484.

Biggs, D.C., Muller-Karger, F.E., 1994. Ship and satellite observations of chlorophyll stocks in warm- and cold-core rings in the western Gulf of Mexico, 7 J. Geophys. Res. 99 (C4), 371–377, 384.

Bleck, R., 2002. An oceanic general circulation model framed in hybrid isopycnic-Cartesian coordinates. Ocean Model. 4 (1), 55–88.

Breaker, B.K., Watson, K.M., Ensminger, P.A., Storm, J.B., Rose, C.E., 2016. Characterization of peak streamflows and flood inundation of selected areas in Louisiana, Texas, Arkansas, and Mississippi from flood of March 2016: U.S. Geological Survey Scientific Investigations Report 2016– 5162, 33.

Brown, A.L., Carpenter, R.C., 2013. Water-flow mediated oxygen dynamics within massive Porites-algal turf interactions. Mar. Ecol. Prog. Ser. 490, 1–10.

Brown, C.A., Huot, Y., Werdell, P.J., Gentili, B., Claustre, H., 2008. The origin and global distribution of second order variability in satellite ocean color and its potential applications to algorithm development. Remote Sens. Environ. 112, 4186–4203. https://doi.org/10.1016/j.rse.2008.06.008.

Conley, D.J., Paerl, H.W., Howarth, R.W., Boesch, D.F., Seitzinger, S.P., Karl, E., Karl, E., Lancelot, C., Gene, E., Gene, E., 2009. Controlling eutrophication: nitrogen and phosphorus. Science 123, 1014–1015.

Dale, V., Bianchi, T., Blumberg, A., Boynton, W., Conley, D.J., Crumpton, W., David, M., Gilbert, D., Howarth, R., Kling, C., Lowrance, R., 2007. Hypoxia in the northern Gulf of Mexico: an update by the EPA science advisory board. In: EPA-SAB-08-003. EPA Science Advisory Board, Washington, DC.

DiMarco, S.F., Reid, R.O., 1998. Characterization of the principal tidal current constituents on the Texas-Louisiana shelf. J. Geophys. Res. 103 (C2), 3093–3109.

DiMarco, S.F., Strauss, J., May, N., Mullins-Perry, R.L., Grossman, E.L., Shormann, D., 2012. Texas coastal hypoxia linked to Brazos River discharge as revealed by oxygen isotopes. Aquat. Geochem. 18 (2), 159–181.

D'Sa, E., Miller, R.L., McKee, B.A., 2007. Suspended particulate matter dynamics in coastal waters from ocean color: application to the northern Gulf of Mexico. Geophys. Res. Lett. 34 (L23611).

Fournier, S., Reager, J.T., Lee, T., Vazquez-Cuervo, J., David, C.H., Gierach, M.M., 2016. SMAP observes flooding from land to sea: the Texas event of 2015. Geophys. Res. Lett. 43 https://doi.org/10.1002/2016GL070821.

Haas, A.F., Smith, J.E., Thompson, M., Deheyn, D.D., 2014. Effects of reduced dissolved oxygen concentrations on physiology and fluorescence of hermatypic corals and benthic algae. PeerJ 2, e235.

Hamilton, P., Berger, T.J., Johnson, W., 2002. On the structure and motions of cyclones in the northern Gulf of Mexico. J. Geophys. Res. 107 (C12).

Hetland, R.D., DiMarco, S.F., 2008. How does the character of oxygen demand control the structure of hypoxia on the Texas–Louisiana continental shelf? J. Mar. Syst. 70 (1), 49–62.

Hickerson, E.L., Schmahl, G.P., Robbart, M., Precht, W.F., Caldow, C., 2008. The State of Coral Reef Ecosystems of the Flower Garden Banks, Stetson Bank, and Other Banks in the Northwestern Gulf of Mexico. The State of Coral Reef Ecosystems of the United States and Pacific Freely Associated States, pp. 189–217.

Hu, C., Muller-Karger, F., 2008. On the connectivity and "black water" phenomena near the FKNMS: a remote sensing perspective. In: Keller, B.D., Wilmot, F.C. (Eds.), 2008. Connectivity: Science, People and Policy in the Florida Keys National Marine Sanctuary. Colloquium Proceedings, 19-21 August 2004, Key West, FL. Marine Sanctuaries Conservation Series NMSP-08-02. U.S. Department of Commerce, National Oceanic and Atmospheric Administration; National Marine Sanctuary Program, Silver Spring, MD, p. 47.

Hu, C., Hackett, K.E., K Callahan, M., Andréfouët, S., Wheaton, J.L., Porter, J.W., Muller-Karger, F.E., 2003. The 2002 ocean color anomaly in the Florida Bight: a cause of local coral reef decline? Geophys. Res. Lett. 30 (3).

Hu, C., Lee, Z., Franz, B., 2012. Chlorophyll a algorithms for oligotrophic oceans: a novel approach based on three-band reflectance difference. J. Geophys. Res. 117 (C1) https://doi.org/10.1029/2011jc007395.

Johnston, M.A., Nuttall, M.F., Eckert, R.J., Blakeway, R.D., Sterne, T.K., Hickerson, E.L., Schmahl, G.P., Lee, M.T., MacMillan, J., Embesi, J.A., 2019. Localized coral reef mortality event at East flower Garden Bank, Gulf of Mexico. Bull. Mar. Sci.

Kourafalou, V.H., Lee, T.N., Oey, L.Y., Wang, J.D., 1996. The fate of river discharge on the continental shelf, 2: transport of coastal low salinity waters under realistic wind and tidal forcing. J. Geophys. Res. 101 (C2), 3435–3455.

Le Hénaff, M., Kourafalou, V.H., 2016. Mississippi waters reaching South Florida reefs under no flood conditions: synthesis of observing and modeling system findings. Ocean Dyn. 66 (3), 435–459.

Lenihan, H.S., Adjeroud, M., Kotchen, M.J., Hench, J.L., Nakamura, T., 2008. Reef structure regulates small-scale spatial variation in coral bleaching. Mar. Ecol. Prog. Ser. 370, 127–141.

Levin, L.A., Ekau, W., Gooday, A.J., Jorissen, F., Middelburg, J.J., Naqvi, S.W.A., Neira, C., Rabalais, N.N., Zhang, J., 2009. Effects of Natural and Human-Induced Hypoxia on Coastal Benthos.

Lowe, R.J., Falter, J.L., 2015. Oceanic forcing of coral reefs. Annu. Rev. Mar. Sci. 7, 43–66.

Morey, S.L., Martin, P.J., O'Brien, J.J., Wallcraft, A.A., Zavala-Hidalgo, J., 2003. Export pathways for river discharged fresh water in the northern Gulf of Mexico. J. Geophys. Res. 108 (C10), 3303.

Muller-Karger, F.E., 2000. The spring 1998 NEGOM cold water event: remote sensing evidence for upwelling and for eastward advection of Mississippi water (or: how an errant LC anticyclone took the NEGOM for a spin). Gulf Mex. Sci. 1, 55–67.

Muller-Karger, F.E., Walsh, J.J., Evans, R.H., Meyers, M.B., 1991. On the seasonal phytoplankton concentration and sea surface temperature cycles of the Gulf of Mexico as determined by satellites. J. Geophys. Res. 96 (C7), 12645–12665.

Muller-Karger, Frank, E., Smith, Joseph P., Werner, Sandra, Chen, Robert, Mitchell, Roffer, Liu, Yanyun, Muhling, Barbara, Lindo-Atichati, David, Lamkin, John, Cerdeira-Estrada, Sergio, Enfield, David B., 2015. Natural variability of surface oceanographic conditions in the offshore Gulf of Mexico. Prog. Oceanogr. https://doi.org/10.1016/j.pocean.2014.12.007.

Nababan, B., Muller-Karger, F.E., Hu, C., Biggs, D.C., 2011. Chlorophyll variability in the northeastern Gulf of Mexico. Int. J. Remote Sens. 32 (23), 8373–8391.

Nakamura, T., Van Woesik, R., 2001. Water-flow rates and passive diffusion partially explain differential survival of corals during the 1998 bleaching event. Mar. Ecol. Prog. Ser. 212, 301–304.

Nakamura, T., Van Woesik, R., Yamasaki, H., 2005. Photoinhibition of photosynthesis is reduced by water flow in the reef-building coral Acropora digitifera. Mar. Ecol. Prog. Ser. 301, 109–118.

Nepf, H.M., 2012. Flow and transport in regions with aquatic vegetation. Annu. Rev. Fluid Mech. 44, 123–142.

Nepf, H.M., Vivoni, E.R., 2000. Flow structure in depth-limited, vegetated flow. J. Geophys. Res. 105 (C12), 28547–28557.

Nowlin, W.D., Jochens, A.E., DiMarco, S.F., Reid, R.O., Howard, M.K., 2005. Low-frequency circulation over the Texas-Louisiana continental shelf. In: Sturges, W., Lugo-Fernandez, A. (Eds.), Circulation in the Gulf of Mexico: Observations and Models. AGU, Washington, D. C, pp. 219–240.

O'reilly, J.E., 2000. Ocean Color Chlorophyll a Algorithms for SeaWiFS, OC2, and OC4: Version 4. SeaWiFS Postlaunch Calibration and Validation Analyses, vol 3, pp. 9–23.

Otis, D.B., 2012. Spatial and temporal variability of remotely sensed ocean color parameters in coral reef regions. Graduate Theses and Dissertations. https://scholarcommons.usf.edu/etd/4379. (Accessed 31 May 2019).

Otis, D.B., Le Hénaff, M., Kourafalou, V.H., McEachron, L., Muller-Karger, F.E., 2019. Mississippi river and campeche bank (Gulf of Mexico) episodes of cross-shelf export of coastal waters observed with satellites. Remote Sens. 11 (6), 723.

Pomeroy, A.W., Lowe, R.J., Ghisalberti, M., Storlazzi, C., Symonds, G., Roelvink, D., 2017. Sediment transport in the presence of large reef bottom roughness. J. Geophys. Res. 122 (2), 1347–1368.

Rabalais, N.N., Turner, R.E. (Eds.), 2001. Coastal Hypoxia: Consequences for Living Resources and Ecosystems. American Geophysical Union, Washington, DC.

Rabalais, N.N., Turner, R.E., Wiseman Jr., W.J., 2002. Gulf of Mexico hypoxia, aka "The dead zone". Annu. Rev. Ecol. Systemat. 33 (1), 235–263.

Schaeffer, B.A., Conmy, R.N., Duffy, A.E., Aukamp, J., Yates, D.F., Craven, G., 2015. Northern Gulf of Mexico estuarine coloured dissolved organic matter derived from MODIS data. Int. J. Remote Sens. 36 (8), 2219–2237.

Schiller, R.V., Kourafalou, V.H., 2010. Modeling River plume dynamics with the HYbrid Coordinate Ocean model. Ocean Model. 33 (1–2), 101–117.

Schmahl, G.P., Hickerson, E.L., Precht, W.F., 2008. Biology and ecology of coral reefs and coral communities in the Flower Garden Banks region, northwestern Gulf of Mexico. Coral Reefs of the USA 221–261.

Soto, I., Andrefouet, S., Hu, C., Muller-Karger, F.E., Wall, C.C., Sheng, J., Hatcher, B.G., 2009. Physical connectivity in the Mesoamerican Barrier Reef System inferred from 9 years of ocean color observations. Coral Reefs. https://doi.org/10.1007/s00338-009-0465-0.

Spalding, M., Bunting, G., 2004. A Guide to the Coral Reefs of the Caribbean. Univ of California Press.

TABS (Texas Automated Buoy System Database), 2018. College station, TX: geochemical and environmental research Group, Texas A&M university; c2018, 14 January, 2017. Available from: http://tabs.gerg.tamu.edu/Tglo. (Accessed 5 June 2019).

Teague, W.J., Wijesekera, H.W., Jarosz, E., Fribance, D.B., Lugo-Fernández, A., Hallock, Z.R., 2013. Current and hydrographic conditions at the east flower Garden Bank in 2011. Cont. Shelf Res. 63, 43–58.

Walker, N.D., Huh, O.K., Rouse Jr., L.J., Murray, S.P., 1996. Evolution and structure of a coastal squirt off the Mississippi River delta: northern Gulf of Mexico. J. Geophys. Res. 101 (C9), 20643–20655.

White, M., Bashmachnikov, I., Arístegui, J., Martins, A., 2007. Physical processes and seamount productivity. Seamounts: ecology, fisheries and conservation 65–84.

Zavala-Hidalgo, J., Gallegos-García, A., Martínez-López, B., Morey, S.L., O'Brien, J.J., 2006. Seasonal upwelling on the western and southern shelves of the Gulf of Mexico. Ocean Dyn. 56 (3), 333–338.

Zavala-Hidalgo, J., Romero-Centeno, R., Mateos-Jasso, A., Morey, S.L., Martínez-López, B., 2014. The response of the Gulf of Mexico to wind and heat flux forcing: what has been learned in recent years? Atmósfera 27 (3), 317–334.

Zhang, W., Hetland, R.D., DiMarco, S.F., Fennel, K., 2015. Processes controlling mid-water column oxygen minima over the Texas-Louisiana shelf. J. Geophys. Res. 120 (4), 2800–2812.